Diffuse X-ray emission in globular cluster cores

C. Y. Hui[1], K. S. Cheng[2], and Ronald E. Taam[3,4,5]

ABSTRACT

The unresolved X-ray emission in the cores of 10 globular clusters hosting millisecond pulsars is investigated. Subtraction of the known resolved point sources leads to detectable levels of unresolved emission in the core region of M28, NGC 6440, M62, and NGC 6752. The X-ray luminosities in the 0.3-8 keV energy band of this emission component were found to lie in the range $\sim 1.5 \times 10^{31}$ ergs s^{-1} (NGC 6752) to $\sim 2.2 \times 10^{32}$ ergs s^{-1} (M28). The lowest limiting luminosity for X-ray source detections amongst these four clusters was 1.1×10^{30} ergs s^{-1} for NGC 6752. The spectrum of the unresolved emission can be fit equally well by a power-law, a thermal bremsstrahlung model, a black body plus power-law, or a thermal bremsstrahlung model plus black body component. The unresolved emission is considered to arise from the cumulative contribution of active binaries, cataclysmic variables, and faint millisecond pulsars with their associated pulsar wind nebulae. In examining the available X-ray data, no evidence for any pulsar wind nebular emission in globular clusters is found. It is shown that the X-ray luminosity contribution of a faint source population based on an extrapolation of the luminosity function of detected point sources is compatible with the unresolved X-ray emission in the cores of NGC 6440 and NGC 6752. Adopting the same slope for the luminosity function for M62 as for NGC 6440 and NGC 6752 leads to a similar result for M62. For M28, the contribution from faint sources in the core can attain a level comparable with the observed value if a steeper slope is adopted. The characteristics on the faint source population as constrained by the properties of the unresolved X-ray emission are briefly discussed.

[1]Max-Planck Institut für Extraterrestrische Physik, 85741 Garching bei München, Germany

[2]Department of Physics, University of Hong Kong, Pokfulam Road, Hong Kong

[3]Department of Physics and Astronomy, Northwestern University, 2131 Tech Drive, Evanston, IL 60208

[4]Academia Sinica Institute of Astronomy and Astrophysics - TIARA, P.O. Box 23-141, Taipei, 10617 Taiwan

[5]Academia Sinica Institute of Astronomy and Astrophysics/National Tsing Hua University - TIARA, Hsinchu, Taiwan

Subject headings: stars: globular clusters: general — x-rays: stars — pulsars: general — x-rays: observations — x-rays

1. INTRODUCTION

The point X-ray source population in globular cluster stellar systems has received much attention in recent years as a direct result of the high angular resolution studies afforded by the Chandra X-ray Observatory. The observational studies have provided an invaluable probe for investigating the binary star population containing compact objects in these systems. For example, the globular clusters with X-ray sources brighter than 4×10^{30} ergs s^{-1} have revealed a strong correlation between the number of such sources with the normalized encounter rate in the cluster (see Pooley et al. 2003) with implications on their formation by dynamical means and on the equilibrium state of the globular cluster systems themselves (Fregeau 2008).

In addition to the studies of the bright X-ray sources, such as low mass X-ray binaries, investigations of the fainter X-ray source population have also revealed important diagnostic information on the importance of dynamical interactions in forming cataclysmic variable stars (Pooley & Hut 2006). Furthermore, the recognition that recycled millisecond pulsars contribute to this faint population (Grindlay et al. 2001) poses important questions regarding their formation, evolution, and retention within the dense stellar environment of globular clusters. In this regard, we note that the observations in the radio wavelength region have been particularly important in characterizing this neutron star subpopulation, with over 140 such radio pulsars now known to be present in globular clusters.

Progress in the theoretical understanding of the formation of compact objects in binary systems within globular clusters has advanced in parallel based on phenemological studies of the importance of dynamical processes in the formation of cataclysmic variables (e.g., Pooley & Hut 2006) and binary population synthesis studies which include stellar dynamical interactions in a model globular cluster system (Ivanova et al. 2007, 2008). An important finding is the realization that the retention of neutron stars in globular clusters may result from the formation of neutron stars via core collapse induced by an electron capture process, confirming an earlier suggestion by Podsiadlowski et al. (2004).

In contrast to the point source population, little work has been directed toward the study of the unresolved faint point source population or diffuse X-ray emission in globular cluster systems. Recently, Okada et al. (2007) have investigated the extended emission in 6

globular clusters, finding evidence for the presence of diffuse emission in 47 Tuc and NGC 6752 offset from the cluster center. The origin of this emission was suggested as resulting from the production of shocks associated with the motion of the globular cluster through the Galactic halo. In this study, we focus on the unresolved or diffuse emission in the high density core regions of globular clusters where the presence of millisecond pulsars (MSPs) suggests that dynamical interactions were important in the formation of these objects as well as of other compact binary systems. The possible existence of such emission, therefore, may reflect a consequential outcome of the formation (and perhaps destruction) of binaries in cluster cores. To assess the contribution of faint X-ray sources such as active binaries, cataclysmic variables, and faint MSPs with their pulsar wind nebulae (PWNe) to the unresolved X-ray emission in the core region, we have carried out an observational investigation to detect the diffuse X-ray emission component in the core region of select globular clusters. In the next section, we present the observations and data analysis of a number of globular clusters which have been studied by the Chandra X-ray Observatory with sub-arcsecond angular resolution so that the diffuse emission can be distinguished from the X-ray point source contribution. Based on the spectral characteristics and luminosity of the unresolved emission in the core region, we examine the potential contribution of unresolved point sources and the diffuse emission of PWNe from MSPs in §3. The implications of our results and suggested follow up observations are discussed in the last section.

2. X-RAY OBSERVATIONS AND DATA ANALYSIS

In order to better isolate the X-ray point sources from the unresolved emission in the cluster cores, our analysis was limited only to the data obtained by the Chandra X-ray Observatory which provides sub-arcsecond angular resolution. Specifically, we have undertaken a systematic search of the Chandra data archive for observations of all globular clusters that belong to the group that host MSPs. Since we are only interested in imaging spectroscopic data, only the data obtained by the Advanced CCD Imaging Spectrometer (ACIS) without any grating was selected. As the regions of interest in our analysis are the cluster cores, only clusters having core radii $r_c \gtrsim 5$", which are sufficiently large for our study, were chosen. Given these selection criteria, 10 globular clusters were selected. The corresponding observational details are summarized in Table 1 and the physical properties of these clusters are summarized in Table 2.

We have deliberately excluded 47 Tucanae and Terzan 5 in this work because the densities of X-ray point sources are very high in these two clusters (cf. Fig. 1 in Heinke et al. 2006 and Fig. 2 in Heinke et al. 2005). The removal of all known point sources in these

clusters resulted in insufficient photons for any detailed analysis.

In our study, standard processed level-2 data were used on the cluster cores (i.e. a circular region with radius of r_c). All the detected point sources were removed within r_c from the data. We simulated the model point spread function (PSF) at 1 keV for the point sources by using MARX. For the inputs of the simulations, we adopted the same roll, off-axis angle, and determined the density of rays by using the effective area of the CCD and the corresponding detected counts for each source. With the consideration of the PSF wings, the excluded regions were optimized so as to mininize the contamination from these discrete X-ray sources in order to retain as many unresolved X-rays in the core region as possible at the same time.

Since our regions of interest were all located on the back-illuminated ACIS-S3 CCD chip which has a superior low energy response, we performed our analysis in the energy band of $0.3 - 8$ keV. The response files were computed by using the tools MKRMF and MKARF in CIAO 3.4. Ultilizing the updated calibration data, CALDB 3.4.1, these files incorporate the corrected degradation for the quantum efficiency in the ACIS CCD. All the spectral fittings were performed with XSPEC 12.3.1, and the quoted errors of the spectral parameters are 1σ for 1 parameter of interest.

2.1. M28 (NGC 6626)

M28 has been observed by Chandra on five occasions. Three were performed with the Advanced CCD Imaging Spectrometer (ACIS-S) and two were carried out with the High Resolution Camera (HRC-S). Since the HRC-S data do not provide any spectral information, we do not consider these datasets in this paper. The ACIS-S observations were scheduled on 4 July 2002, 4 August 2002 and 9 September 2002 with an effective exposure of $\sim 13 - 14$ ks (Table 1). Using these datasets, Becker et al. (2003) detected 46 discrete X-ray point sources in total by means of a wavelet detection algorithm. We have re-run the source detection on the merged data and independently confirmed the results reported by Becker et al. (2003). On the basis of the detection limit, a limiting luminosity at a level of $\sim 3.5 \times 10^{30}$ ergs s^{-1} is inferred (see the last column in Table 2). The emission properties of these point sources have been characterized by Becker et al. (2003) and Becker & Hui (2007), and include the X-ray counterparts of MSPs M28A and M28H.

With a view to obtain better statistics for the analysis, all ACIS observations were combined to produce improved images. Prior to the merging process, the aspect offsets for each observation, which is a function of the spacecraft roll angle, have been carefully

checked and corrected. All three datasets were then merged to a common position. After the subtraction of all known point sources, we estimated that the total contribution of the PSF wings centered on these sources in the remaining photons should be $\sim 10\%$. The contamination is dominated by the pulsar M28A and the brightest source in the field (source #26 in Tab. 3 of Becker et al. 2003), which was identified as a quiescent low mass X-ray binary candidate.

We also estimated the possible contribution of background sources within r_c. By fitting the projected surface density of M28, Becker et al. (2003) obtained the best-fitted value of 0.36 ± 0.22 background sources per arcmin^2. This is comparable with the estimate from the Chandra Deep Field South (Rosati et al. 2002). Assuming the background sources are uniformly distributed, we conclude that the contribution of background sources in our region of interest is negligible.

The raw X-ray image of the unresolved emission from the cluster core (i.e. a circular region of interest with $r = r_c$) is shown in Figure 1. The image is binned with a factor of 0.5 arcsec. The radio timing positions of eight MSPs in this field of view are illustrated as crosses in Figure 1 (cf. Tab. 2 in Becker & Hui 2007). We notice that two clumps of photons are close to the timing positions of MSPs M28G and M28J. While the feature near M28J is adjacent to the subtracted region of a detected source and thus can possibly be a result arising from the imperfect subtraction, the clump close to M28G is likely to be a faint source just below the detection limit of resolved sources.

We have also computed the surface brightness profile of the unresolved emission in M28 which is displayed in Figure 2. Comparing this profile with the best-fit projected surface density $S(r)$ of the detected X-ray point sources in the cluster (cf. Becker et al. 2003), we notice that the best-fit $S(r)$ (solid line in Fig.2) falls much slower than the brightness profile of the unresolved emission. Within 1σ errors of the parameters in $S(r)$ reported by Becker et al. (2003) (dotted line in Fig.2), the radial profile of the unresolved emission has a similar trend as that of the detected point sources. A comparison with radial distributions of different populations of X-ray emitting objects (e.g. white dwarfs and MSPs) may provide insights into the nature of the unresolved X-ray emission.

The spectrum of the diffuse emission in all datasets was extracted from a circle of $r = r_c$ centered on the cluster center. In addition, the background spectrum was extracted from a source free region within a 10 arcsec radius centered at RA=$18^{\rm h}24^{\rm m}32.209^{\rm s}$, Dec=$-24°51'46.11$" (J2000). After background subtraction, there are totally 259 ± 16 net counts available for the spectral analysis. The background contribution was estimated to be $\sim 15\%$. The net counting rates for the observations in July, August and September are $(6.4\pm0.8)\times10^{-3}$ cts/s, $(5.2\pm0.8)\times10^{-3}$ cts/s, and $(6.4\pm0.9)\times10^{-3}$ cts/s. Each spectrum was

dynamically binned so as to have at least 10 counts per bin. To better constrain the spectral properties, we fitted the spectra obtained from all observations simultaneously. Four different spectral models were adopted, corresponding to a power-law, thermal bremsstrahlung, power-law plus black body, and thermal bremsstrahlung plus black body. The results are summarized in Table 3.

We found that a power-law model fits the data reasonably well ($\chi^2_\nu = 0.83$ for 25 D.O.F.). This model yields a column density of $n_H = 2.75^{+0.78}_{-0.84} \times 10^{21}$ cm^{-2} and a photon index of $\Gamma = 2.35^{+0.41}_{-0.25}$. The energy spectrum is displayed in Figure 3. No systematic deviation of the fitting residual is found for the absorbed power-law model in $0.3 - 8$ keV (see lower panel of Fig. 3). At a distance of 5.5 kpc, the unabsorbed luminosity deduced from this model is $L_X = 2.54^{+1.27}_{-0.62} \times 10^{32}$ erg s^{-1} in the energy range of $0.3 - 8$ keV. In addition to the power-law model, we found that the thermal bremssstrahlung model can describe the data equally well ($\chi^2_\nu = 0.82$ for 25 D.O.F.) with $n_H = 1.50^{+0.90}_{-0.76} \times 10^{21}$ cm^{-2} and a temperature of $kT = 2.58^{+1.09}_{-0.75}$ keV. This best-fit model implies an absorption-corrected luminosity of $L_X = 1.67^{+0.99}_{-0.62} \times 10^{32}$ erg s^{-1} at 5.5 kpc. The best-fit values of n_H in both these models are consistent with that deduced from the foreground reddening (i.e. $\sim 2.2 \times 10^{21}$ cm^{-2}).

Since the X-ray emission from most of the MSPs detected in 47 Tuc is thermally dominant (Bogdanov et al. 2006), it is instructive to examine the possible contribution of a MSP population by including a black body component despite the fact that the single component of power-law/thermal bremsstrahlung model can well describe the data already. To better constrain the contribution of the black body component, we fixed n_H at the value deduced from the optical reddening and the black body temperature at 2.1×10^6 K which is the mean value inferred from the MSP population in 47 Tuc (Bogdanov et al. 2006). Acceptable fits were found, resulting in a black body contribution of $\lesssim 9\%$ and $\sim 12\%$ in the power-law plus black body (PL+BB) and the thermal bremsstrahlung plus black body (BREMSS+BB) fits respectively.

The robustness of the best-fitted parameters quoted in this paper were checked by repeating all the aforementioned spectral fitting by incorporating the background spectrum extracted from different source-free regions in the observed data as well as the ACIS "blank sky" background files. It is found that within 1σ errors the spectral parameters inferred from independent fittings are all consistent with each other.

2.2. NGC 6440

NGC 6440 has been observed by the Chandra X-ray Observatory on three occasions (see Table 1). All the observations were carried out by ACIS-S and scheduled on 4 July 2000, 13 August 2001 and 27 June 2003 respectively. Using the data obtained from the observation on 4 July 2000, Pooley et al. (2002) detected 24 discrete X-ray point sources to a limiting luminosity of $\sim 2 \times 10^{31}$ ergs s^{-1} within the half-mass radius (cf. Table 2 in Pooley et al. 2002), 16 of which are located inside the core radius. The source CX 1 as listed in the Table 2 of Pooley et al. (2002) has been identified as an X-ray transient (in 't Zand et al. 2001). While NGC 6440 was observed on 4 July 2000 when CX 1 was quiescent, a target-of-opportunity (TOO) observation on 13 August 2001 detected an outburst from a transient with a luminosity of $\sim 9 \times 10^{35}$ ergs s^{-1} (in 't Zand et al. 2001). Owing to the outburst, the data obtained from the TOO observation were seriously compromised by pileup effects. Therefore, we do not include this dataset in the subsequent analysis.

The observations on 4 July 2000 and 27 June 2003 have an effective exposure of ~ 23 ks and ~ 24 ks respectively. Aspect offsets have been carefully checked and corrected for each dataset. As our primary interest is the unresolved X-rays in the cluster core, we first removed all the 16 resolved point sources within r_c from the data. After excluding the contributions from the point sources as reported in Table 2 in Pooley et al. (2002), we compared the count rates of the residual emission within r_c from both observations. We noticed that the net count rate in the 2003 observation is higher than that of the 2000 observation at a level of $\sim 3\sigma$.

This led to a closer inspection of both datasets, and images were produced with a bin-size of 0.5 arcsec from both observations. Applying the wavelet source detection algorithm on each image individually, an additional source, besides the point sources reported by Pooley et al. (2002), was detected close to the cluster center in the 2003 observation. This source is located at RA=$17^{\rm h}48^{\rm m}52.656^{\rm s}$, Dec=$-20^\circ21'34.25"$ (J2000). On the other hand, with the same detection algorithm, the source was not detected in the 2000 observation. This led to the detection of a new transient X-ray source in NGC 6440. The background subtracted count rates of the X-ray transient are $(2.07 \pm 0.96) \times 10^{-4}$ cts/s and $(1.03 \pm 0.21) \times 10^{-3}$ cts/s in 2000 observation and 2003 observation respectively. The significance of the difference in count rates is at a level of $> 3\sigma$.

Since a new source is detected in the core of NGC 6440, in addition to the sources reported by Pooley et al. (2002), we further subtracted its contribution in both datasets. After removing all the known point sources, the total contribution of the PSF wings centered on these point sources in the remaining photons within the core was estimated to be $\sim 18\%$. The net count rates of the unresolved X-ray emission within r_c are $(1.15 \pm 0.24) \times 10^{-3}$ cts/s

and $(1.13 \pm 0.24) \times 10^{-3}$ cts/s for the 2000 observation and 2003 observations respectively. Thus, the count rates from both observations are fully consistent with each other, and the lack of variability justifies combining both datasets to improve the photon statistics.

We extracted the spectrum of the unresolved X-ray emission in both datasets from a circle of $r = r_c$ centered on the cluster center. The background spectrum was extracted from a source free region within a 10 arcsec radius centered at RA=$17^{\rm h}48^{\rm m}54.324^{\rm s}$, Dec=$-20°21'25.80$" (J2000). After background subtraction, there are totally 54 ± 7 net counts available for the spectral analysis. The background contribution was estimated to be $\sim 11\%$. Each spectrum was dynamically binned so as to have at least 10 counts per bin. We fitted both spectra simultaneously to better constrain the spectral properties.

In view of the limited photon statistics, we fixed the column density at the reddening inferred value (i.e. $n_H = 5.9 \times 10^{21}$ cm^{-2}) for all the spectral fits. A power-law model can describe the data fairly well ($\chi^2_\nu = 0.39$ for 4 D.O.F.) which yields a photon index of $\Gamma = 2.04^{+0.50}_{-0.46}$ and an unabsorbed luminosity of $L_X = 2.00^{+1.71}_{-0.76} \times 10^{32}$ erg s^{-1} in the $0.3 - 8$ keV energy band. A thermal bremsstrahlung model can also describe the data ($\chi^2_\nu = 0.44$ for 4 D.O.F.), yielding a temperature of $3.06^{+6.18}_{-1.25}$ keV and an unabsorbed luminosity of $L_X = 1.57^{+1.51}_{-0.74} \times 10^{32}$ erg s^{-1}.

Following the procedure described in §2.1, we have also estimated the possible contribution of a faint MSP population in NGC 6440 by incorporating a black body component in the spectral fits. This spectral component is found to contribute $\sim 17\%$ and $\sim 7\%$ in the PL+BB and BREMSS+BB fits respectively.

2.3. M62 (NGC 6266)

M62 was observed on 12 May 2002 with ACIS-S. The effective exposure of this observation was ~ 62 ksec. Using this data, Pooley et al. (2003) detected 51 X-ray point sources within a half-mass radius of $1'.23$. However, the details of these X-ray sources have not been reported in the literature. We have independently performed the source detection. Using a wavelet detection algorithm, we have detected 12 discrete sources within r_c at a detection limit of $\sim 7 \times 10^{30}$ erg s^{-1}.

After the removal of all detected point sources in the core, we estimated that the total contribution of the PSF wings centered on these point sources in the remaining photons is about 20%.

The spectrum of the unresolved X-ray emission in both datasets was extracted from

a circle of $r = r_c$ centered on the cluster center. The background spectrum was extracted from a source free region within a 10 arcsec radius centered at RA=$17^{\rm h}01^{\rm m}10.610^{\rm s}$, Dec=$-30°06'27.63$" (J2000). After background subtraction, 164 ± 13 net counts were available for the spectral analysis. The background contribution is rather small which was estimated to be $\sim 5\%$. The spectrum was dynamically binned so as to have at least 15 counts per bin.

A power-law model can describe the data very well ($\chi^2_\nu = 0.43$ for 8 D.O.F.). In this case, the best-fitted model yields a hydrogen column density of $n_H < 5.19 \times 10^{20}$ cm^{-2}, a photon index of $\Gamma = 1.54^{+0.22}_{-0.16}$ and an unabsorbed luminosity of $L_X = 1.50^{+0.62}_{-0.36} \times 10^{32}$ erg s^{-1} in the $0.3 - 8$ keV energy band. The inferred n_H is small in comparison with the value inferred from the average reddening (i.e. $n_H = 2.6 \times 10^{21}$ cm^{-2}). However, this does not invalidate the spectral results reported here as the reddening across the cluster is found to be highly varied (Possenti et al. 2003; Minniti, Coyne, & Claria 1992). We have also attempted to fix n_H at the value inferred by the average reddening, however, the power-law model was not found to describe the data below 1 keV and above 3 keV, resulting in a worse goodness-of-fit ($\chi^2_\nu = 1.03$ for 9 D.O.F.).

The thermal bremsstrahlung model can also describe the data with a comparable goodness-of-fit ($\chi^2_\nu = 0.58$ for 8 D.O.F.). This best-fit model also yields a rather low column density of $n_H < 3.48 \times 10^{20}$ cm^{-2} with a temperature of $kT = 9.23^{+17.50}_{-4.10}$ keV and an unabsorbed luminosity of $L_X = 1.41^{+0.26}_{-0.27} \times 10^{32}$ erg s^{-1} in the $0.3 - 8$ keV energy band.

In the PL+BB and BREMSS+BB fits, the black body component with the temperature fixed at 2.1×10^6 K is found to contribute $\sim 35\%$ and $\sim 32\%$ respectively.

2.4. NGC 6752

NGC 6752 was observed by the Chandra X-ray Observatory on two occasions (see Table 1). All the observations were carried out by ACIS-S and scheduled on 15 May 2000, and 10 February 2006. Using the data obtained from the observation on 15 May 2000, Pooley et al. (2002b) detected 19 discrete X-ray point sources within the half-mass radius (cf. Table 1 in Pooley et al. 2002b). We have re-analysed the X-ray image of the cluster by combining both observations and inferred a limiting luminosity of 1.1×10^{30} ergs s^{-1}. Nine of the resolved X-ray sources are located inside the core radius. After removing these point sources, we estimate that the total contribution of the PSF wings centered on these sources in the remaining unresolved photons is about 25%.

We extracted the spectrum of the unresolved X-ray emission in both datasets from

a circle of $r = r_c$ centered on the cluster center. The background spectrum was extracted from a source free region within a 10 arcsec radius centered at RA=$19^{\rm h}10^{\rm m}47.967^{\rm s}$, Dec=$-59°59'05.36$" (J2000). The background subtracted count rates for the observations in 2000 and 2006 are $(1.06 \pm 0.23) \times 10^{-3}$ cts/s and $(0.95 \pm 0.20) \times 10^{-3}$ cts/s. The count rates from both observations are thus consistent with each other within 1σ and justifies combining both datasets to improve the photon statistics. After background subtraction, 67 ± 8 net counts were available for the spectral analysis. The background contribution was estimated to be $\sim 26\%$. The spectrum was dynamically binned so as to have at least 10 counts per bin.

In view of the limited photon statistics, we fixed the column density at the reddening inferred value, i.e. $n_H = 2.2 \times 10^{20}$ cm^{-2}. A power-law model can provide a reasonable description of the data ($\chi^2_\nu = 0.95$ for 7 D.O.F.). The best-fit model yields a photon index of $\Gamma = 1.94^{+0.39}_{-0.36}$ and an unabsorbed luminosity of $L_X = 1.50^{+0.75}_{-0.42} \times 10^{31}$ erg s^{-1} in $0.3 - 8$ keV. Fitting the data with a thermal bremsstrahlung model also results in a good description ($\chi^2_\nu = 0.89$ for 7 D.O.F.) resulting in a temperature of $2.38^{+3.06}_{-1.00}$ keV and an unabsorbed luminosity of $L_X = 1.19^{+1.12}_{-0.56} \times 10^{31}$ erg s^{-1}. In the PL+BB and BREMSS+BB fits, the black body component with the temperature fixed at 2.1×10^6 K is found to contribute $\lesssim 15\%$ and $\lesssim 28\%$ respectively.

2.5. Other clusters

For the other selected globular clusters, no conclusive evidence for an excess of unresolved X-ray emission in their cores is found. After removing all the resolved X-ray point sources, we found that the background contributions in the remaining photons within these cluster cores are $\gtrsim 65\%$.

3. NATURE OF THE UNRESOLVED CORE X-RAY EMISSION

To probe the physical nature of the unresolved X-ray emission in the cores of globular clusters, there are two possibilities to consider. Namely, the emission is simply a superposition of unresolved faint X-ray point sources or the observed X-rays can be diffuse in origin. We discuss each of these possibilities in turn.

3.1. Unresolved point sources

Various classes of faint X-rays objects have been identified in globular clusters, including quiescent low mass X-ray binaries (qLMXBs), MSPs, cataclysmic variables (CVs), and the chromospherically active main sequence binaries (ABs). Although the individual contribution of these classes of systems at the low limiting luminosities ($< L_{\rm limit}$) of our study are unknown, we examine the possibility that the detected residual X-ray emission in the cluster cores is a result of a blend of faint X-ray sources following the method used by Okada et al. (2007). Specifically, we assume a cumulative luminosity function of the form $N(> L_X) = N_0 L_X^{-q}$ and its extrapolation to luminosities, L_X, below $L_{\rm limit}$. The normalization N_0 can be determined from the local source number density of X-ray sources above $L_{\rm limit}$ in each cluster core. The slope q has been inferred to be 0.5 in both NGC 6440 and NGC 6752 by Pooley et al. (2002), but has not been determined for M28 and M62. Here, we assume it to be 0.5 in these two clusters as well.

With the aforementioned assumptions, the contribution from the faint X-ray source population below the detection threshold is estimated to be 4.1×10^{31} erg s^{-1}, 3.1×10^{32} erg s^{-1}, 8.5×10^{31} erg s^{-1}, and 1.0×10^{31} erg s^{-1} in the cores of M28, NGC 6440, M62 and NGC 6752 respectively. The estimates for NGC 6440 and NGC 6752 are within the 1σ uncertainities and for M62 within the 2σ uncertainty of the corresponding observed unresolved X-ray luminosities. On the other hand, the contribution from unresolved sources in M28 is about ~ 5 times smaller than the observed value. We note, however, that this preliminary result is sensitive to the adopted slope of the luminosity function. For example, for a slope as steep as that inferred in the case of 47 Tuc (i.e. $q = 0.78$ Pooley et al. 2002), the total luminosity of the unresolved point source population in M28 can attain a level ($\sim 1.5 \times 10^{32}$ s^{-1}) comparable to its observed value. Adopting such a slope for M62 similarly leads to a higher contribution corresponding to unresolved X-ray luminosity of 3.0×10^{32} s^{-1}, which is close to the 1σ uncertainty of the observed value. Hence, notwithstanding the spectral properties of the unresolved emission, which depend on the relative contribution of each sub population, the luminosity level of the residual X-ray emission found in the cores of these globular could reflect the contribution of unresolved faint sources, subject to our choice for extrapolation of the luminosity function to luminosities less than $L_{\rm limit}$.

3.2. Diffuse emission

In view of the uncertainties in the estimates of the contribution of a faint point source population to the unresolved X-ray emission, we also consider the possibility that the emission is diffuse in origin. In this case, we explore the hypothesis that the high energy emission

with photon energy higher than several keV results from PWNe of MSPs. The outflow accompanying their relativistic winds could be responsible for reducing the amount of intracluster gas in the clusters (see Spergel 1991). Indeed, the low dispersion measure for the pulsars in 47 Tuc (Freire et al. 2001) suggests that some mechanism operates to reduce the mass of gas in the central region expected to be accumulated in the $\sim 10^7 - 10^8$ year interval between passages of the cluster through the Galactic disk (cf. Camilo & Rasio 2005).

It is known that globular clusters of high central densities host a large number of MSPs (e.g. 47 Tuc, Terzan 5). Based on the results of §2, the limiting luminosities for point source detection in the four globular clusters with sufficient photons for spectral analysis are in the range $1.1 - 18 \times 10^{30}$ergs s^{-1}, which overlaps with the range of luminosities found for most MSPs in 47 Tuc ($\sim 1 - 4 \times 10^{30}$ ergs s^{-1}; Grindlay et al. 2002). In addition, the spectra of MSPs in 47 Tuc are mainly thermal with a black body temperature $kT \sim 0.2$ keV. If we assume that the black body luminosity component obtained by fitting the model of PL+BB listed in Table 3 results from unresolved MSPs and the limiting luminosity listed in Table 2 is the upper limit of the characteristic luminosity of the unresolved MSPs in various globular clusters, the possible number of faint MSPs in the core regions of M28, NGC 6440, M62 and NGC 6752 could be 6, 2, 12 and 2 respectively.

It is of some interest to compare these estimates with the uncovered pulsar population in each cluster core. In the case of M28, there are 6 MSPs located within one core radius after the exclusion of M28A (cf. Fig. 1). For NGC 6440 and NGC 6752, the radio timing positions of MSPs NGC 6440B and NGC 6752D are found to coincide with the X-ray sources in their cores (cf. Hui et al. 2009). Therefore, their X-ray contribution has already been removed in the procedure of PSF subtraction. After excluding these two MSPs, there are 2 MSPs in each of these two cluster cores. Hence, the estimated numbers of MSPs based on the black body components in our PL+BB fittings are comparable with the known MSP population in the cores of these globular clusters.

In M62, 6 MSPs have so far been discovered (D'Amico et al. 2001; Possenti et al. 2003; Chandler 2003). However, timing solutions have only been reported for M62A, M62B and M62C (See Table 1 in Possenti et al. 2003). M62B and M62C are located within one core radius. Since both have identified X-ray counterparts (cf. Hui et al. 2009), their contributions have been removed. Hence, our simple estimate suggests that a potentially additional population of MSPs in the core of M62 may not have been revealed in a previous radio survey. This inference is not unreasonable as the stellar encounter rate in its core is comparable with that of 47 Tuc (cf. Fregeau 2008). On the other hand, the black body component of the unresolved emission can also result from other source classes, such as ABs.

If MSPs in the core contribute to the black body component in the PL+BB fittings, the

power-law component may arise from PWNe in which non-thermal emission emanates from the shock region formed by the interaction of the pulsar wind with the interstellar medium (e.g. Chevalier 2000; Cheng, Taam and Wang 2004, 2006). Adopting a characteristic spin-down power of 10^{34} ergs s^{-1} for the unresolved MSPs, the non-thermal X-ray luminosity contributed by each PWN is estimated to be $\sim 10^{31}$ergs s^{-1} (see Cheng, Taam & Wang 2004). For the estimated number of unresolved MSPs from the thermal component (see above), the total non-thermal luminosities from M28, NGC 6440, M62 and NGC 6752 are 6×10^{31}ergs s^{-1}, 2×10^{31} ergs s^{-1}, 1.2×10^{32} ergs s^{-1}, and 2×10^{31} ergs s^{-1}, respectively. In comparing these model predicted luminosities with the observed luminosities in Table 3, we find that the model predicted non-thermal emission from PWNe is substantially less than the observed diffuse power-law component in M28 and NGC 6440. This implies that the power-law component in these two globular clusters are likely contributed by other subpopulations (e.g., CVs and ABs). On the other hand, the model predicted non-thermal luminosities of M62 and NGC 6752 are comparable to the luminosities in the power-law component in these two globular clusters, suggesting that in this interpretation MSPs may contribute in these two globular clusters. However, the fitted PL index obtained in M62 is near unity, which is a difficulty for the interpretation since the PL index resulting from the PWN emission should exceed 1.5. Taking into account the case of NGC 6752, where the black body luminosity is only an upper limit, we conclude that the evidence for non-thermal emission from PWNe in globular clusters is lacking.

We have further examined this inference by investigating the vicinity of M28A, which is the most powerful one among all the MSPs residing in globular clusters. The emission of PWN mainly arises from a region near the shock radius. Therefore, we calculate the shock radius of M28A by $R_s = (\dot{E}/2\pi\rho v_p^2 c)^{1/2} \sim 5 \times 10^{16} \dot{E}_{34}^{1/2} n_{0.1}^{-1/2} v_{p,2}^{-1}$ cm, where $v_{p,2}$ is the pulsar velocity in units of 100 km s^{-1}, $\dot{E}_{34}$ is the characteristic spin-down power in units of 10^{34} ergs s^{-1}, and $n_{0.1}$ is the number density of the intracluster medium in units of 0.1 cm^{-3} (see Cheng, Taam & Wang 2004). The number density in the core of M28 is estimated as $n \sim \langle DM \rangle / \langle d_\perp \rangle \sim 3.6$ cm^{-3}, where $\langle DM \rangle$ and $\langle d_\perp \rangle$ are the standard deviations of the dispersion measure and the offset of the MSPs in the cluster core (cf. Bégin 2006). Adopting v_p to be the velocity dispersion, $\sqrt{3}\sigma_v = 28$ km/s at the cluster center (where σ_v is the one-dimensional velocity dispersion at the center of M28 [6]), the spin-down power of M28A implies the shock radius to be ~ 5.4 arcsec at 5.5 kpc. This is larger than the region adopted in subtracting the point source contribution at the position of M28A. However, we do not identify any feature around this subtraction region in examining the residual emission (cf. Fig. 1). Therefore, the absence of any extended structure around the powerful MSP

[6] http://www-int.stsci.edu/∼ognedin/gc/vesc.dat

M28A provides further support that there is no compelling evidence for PWNe in globular clusters.

4. DISCUSSION

An observational investigation of the unresolved X-ray emission component in the cores of globular clusters that host MSPs has been carried out. Our sample contains only globular clusters targeted by the Chandra X-ray Observatory in order to take advantage of its sub-arcsecond resolution which is necessary for accurate extraction of the point source contributions to the X-ray emission. The subtraction of known as well as newly discovered X-ray point sources was performed to estimate the luminosity and spectral properties of the unresolved emission. Of the ten globular clusters selected (whose cores are sufficiently large), but excluding 47 Tuc and Terzan 5, detectable unresolved X-ray emission was found for M28, NGC 6440, M62, and NGC 6752. The luminosities in the 0.3-8 keV energy band ranged by about an order of magnitude from $\sim 1.5 \times 10^{31}$ ergs s^{-1} to $\sim 2.5 \times 10^{32}$ ergs s^{-1}. Among these clusters, the limiting luminosity for the point X-ray source detections is as low as 1.1×10^{30} ergs s^{-1} for NGC 6752. The spectra of the unresolved emission were found to be equally well fit, which varied from cluster to cluster, by a power-law characterized by a photon index, Γ, $\sim 1.5 - 2.3$, by a thermal bremsstrahlung model with temperature of $\sim 2 - 9$ keV, or a black body of 0.18 keV plus power-law component ($\Gamma \sim 1 - 2$).

To assess the contribution to the X-ray luminosity in the 0.3-8 keV energy band by faint point sources in these cluster cores, estimates were based on an extrapolation of the luminosity function of detected pointed X-ray sources. We note that these contributions represent a heterogenous stellar population consisting of ABs, CVs, and MSPs. Inherent uncertainties exist in such a procedure since other source populations may contribute at lower luminosities that do not significantly contribute at higher luminosities. Given these caveats, it has been shown that the contribution of a faint source population (with luminosities less than the detection threshold for point sources) can be comparable to the unresolved X-ray emission measured in the cores of NGC 6440, M62, and NGC 6752. On the other hand, the contribution of faint sources to the unresolved emission in M28 can be ~ 5 times less than the measured value, although taking the steeper slope for the X-ray luminosity function of 47 Tuc leads to a faint source contribution comparable to that measured for the unresolved X-ray emission.

Although luminous X-ray PWNe have been detected from pulsars in the field, we do not find any evidence of a PWNe contribution to the diffuse X-ray emission in the globular clusters studied in this paper. This may suggest that the X-ray emission from PWNe is in

slow cooling region, which has a much lower efficiency. However, we have concluded that the diffuse X-ray emission results from the unresolved faint point source population in the cluster cores. In the following, we briefly discuss the characteristics of the faint source population as constrained by the properties of the unresolved X-ray emission.

A number of possible candidate sources could contribute at the faint luminosity levels. Among them are white dwarfs, either magnetic or non-magnetic. For the non-magnetic white dwarfs, X-ray emission could be associated with a boundary layer between the inner edge of the accretion disk and the white dwarf surface. Based on the work by Pandel et al. (2005) of low accretion rate CVs, these sources should be detectable as resolved point sources ($> 10^{31}$ ergs s^{-1} corresponding to accretion rates $> 10^{-12} M_{\odot}$ yr^{-1}). To contribute to the unresolved source population, one requires even lower accretion rates. In contrast, it is more likely that a sub population of magnetic white dwarfs may contribute. For example, low accretion rate polars corresponding to magnetic white dwarfs in detached systems (which capture a substantial fraction of the stellar wind of its detached companion) may be a viable population each contributing at a level of $\sim 10^{30}$ ergs s^{-1} (see Webbink & Wickramasinghe 2005). On the other hand, the white dwarfs in binaries known as polars or intermediate polars, where the mass transfer is accomplished via Roche lobe overflow, which are generally characterized by a hard spectrum with a photon indices near unity (see Heinke et al. 2008), are sufficiently luminous ($> 10^{31}$ ergs/s) that they would have been detected as resolved point sources.

Coronal emission from single stars or ABs is another possible contributor to the faint X-ray emission; however, these sources are generally soft. Harder spectra, corresponding to higher coronal temperatures, are observed from such a population, but at luminosities such that they would be individually detectable (see Güdel 2004). Although strong flares can produce hard spectra, it is difficult to quantify their contribution since the time averaged luminosities of such sources is not well characterized.

Independent estimates of a possible undetected MSP population can be provided by radio data. We have examined the NRAO/VLA Sky Survey image of the field around M28 and found that there is an excess near the center of M28 (see Figure 4). Here, the overlaid contours were computed at the levels between 0.5 mJy/beam−2 mJy/beam. The radio timing positions of all the pulsars within the half-mass radius are illustrated for reference in Figure 4 as crosses, which are all found to have a good correspondence with the radio feature. The FWHM of the feature is ~ 40 arcsec is comparable with the angular resolution of NVSS data (cf. Condon et al. 1998). Assuming a beam size (FWHM) of 45 arcsec, the flux density of this feature is found to be ~ 2.2 mJy. This compares to the sum of the flux densities of the known MSPs ~ 1.5 mJy (Bégin 2006). Since the rms brightness fluctuation of the NVSS

image is at the level of ~ 0.45 mJy/beam (Condon et al. 1998), we cannot determine the possible contribution from the undetected MSPs on the basis of the NVSS data. A sensitive radio inteferometric observation (e.g. ATCA), which can attain a sensitivity limit at the order of ~ 0.01 mJy/beam, is highly desirable to provide a tight independent constraint on the MSP population in this cluster.

We have also searched for radio emission from NGC 6440, M62 and NGC 6752 from the NVSS data and the Sydney University Molonglo Sky Survey (SUMSS) data (Bock et al. 1999), but did not identify any excess near their cores.

Future observations of the core regions of globular cluster systems at fainter limiting X-ray luminosities will be necessary to quantify the luminosity function at lower levels to help distinguish the various subpopulation contributions to the unresolved emission. If additional millisecond pulsars are to contribute to the X-ray emission, improved determinations of the radio timing positions of known MSPs are essential. Such a multi-wavelength observational program is of paramount importance in further constraining the nature and evolutionary history of the faint X-ray point source population in these dense stellar systems.

CYH and KSC were supported by the Croucher Foundation Postdoctoral Fellowship and a GRF grant of Hong Kong Government under HKU700908P respectively. RET was supported in part by the Theoretical Institute for Advanced Research in Astrophysics (TIARA) operated under the Academia Sinica Institute of Astronomy & Astrophysics in Taipei, Taiwan.

REFERENCES

Becker, W., & Hui, C. Y. 2007, arXiv:0705.0119

Becker, W., Swartz, D., Pavlov, G., Elsner, R., Grindlay, J., et al., 2003, ApJ, 594, 798

Bégin, S. 2006, Ph.D. thesis, University of British Columbia

Bock, D. C.-J., Large, M. I., & Sadler, Elaine M. 1999, AJ, 117, 1578

Bogdanov, S., Grindlay, J. E., Heinke, C. O., Camilo, F., Freire, P. C. C., & Becker, W. 2006, ApJ, 646, 1104

Camilo, F. & Rasio, F. A. 2005, in Binary Radio Pulsars, ASP Conf. Proc, Vol. 328, 147

Chandler, A. M. 2003, Ph.D. thesis, California Institute of Technology

Cheng, K.S., Taam, R.E., & Wang, W. 2006, ApJ, 641, 427

Cheng, K. S., Taam, R. E., & Wang, W., 2004, ApJ, 617, 480

Chevalier, R. A. 2000, ApJ, 539, L45

Condon, J. J., Cotton, W. D., Greisen, E. W., Yin, Q. F., Perley, R. A., Taylor, G. B., & Broderick, J. J. 1998, AJ, 115, 1693

D'Amico, N., Lyne, A. G., Manchester, R. N., Possenti, A., & Camilo, F. 2001, ApJ, 548, L171

Fregeau, J. M. 2008, ApJ, 673, L25

Freire, P. C., Kramer, M., Lyne, A. G., Camilo, F., Manchester, R. N., & D'Amico, N. 2001, ApJ, 557, L105

Grindlay, J. E., Heinke, C., Edmonds, P. D., & Murray, S. S. 2001, Science, 292, 5525

Grindlay, J. E., Camilo, F., Heinke, C. O., Edmonds, P. D., Cohn, H., & Lugger, P. 2002, ApJ581, 470

Güdel, M. 2004, A&ARv, 12, 71

Harris, W.E. 1996, AJ, 112, 1487

Heinke, C. O., Ruiter, A. J., Muno, M. P., & Belczynski, K. 2008, astro-ph 0801.1279

Heinke, C. O., Wijnands, R., Cohn, H. N., Lugger, P. M., Grindlay, J. E., Pooley, D., & Lewin, W. H. G. 2006, ApJ, 651, 1098

Heinke, C. O., Grindlay, J. E., Edmonds, P. D., Cohn, H. N., Lugger, P. M., Camilo, F., Bogdanov, S., & Freire, P. C. 2005, ApJ, 625, 796

Hui, C. Y., Huang, H. H., & Becker, W. 2009, submitted to A&A

in't Zand, J. J. M., van Kerkwijk, M. H., Pooley, D., Verbunt, F., Wijnands, R., & Lewin, W. H. G 2001, ApJ, 563, L41

Ivanova, N., Heinke, C.O., Rasio, F.A., Belczynski, K., & Fregeau, J. 2008, MNRAS, 386, 553

Ivanova, N., Heinke, C.O., & Rasio, F.A. 2007, in 40 Years of Pulsars: Millisecond Pulsars, Magnetars, and More AIP Conf. Proc., Vol, 983, 442

Manchester, R. N., Hobbs, G. B., Teoh, A., & Hobbs, M. 2005, AJ, 129, 1993 (for recent update, please refer to http://www.atnf.csiro.au/research/pulsar/psrcat)

Minniti, D., Coyne, G. V., & Claria, J. J. 1992, AJ, 103, 871

Okada, Y, Kokubun, M., Yuasa, T., & Makishima, K. 2007, PASJ, 59, 272

Pandel, D., Cordova, F., Mason, K. O., & Priedhorsky, W. C. 2005, ApJ, 626, 396

Podsidlowski, Ph., Langer, N. Poelarends, A.J.T., Rappaport, S., Heger, A., & Pfahl, E. 2004, ApJ, 612, 1044

Possenti, A., D'Amico, N., Manchester, R. N., Camilo, F., Lyne, A. G., Sarkissian, J., & Corongiu, A. 2003, ApJ, 599, 475

Pooley, D., et al. 2003, ApJ, 591, L131

Pooley, D., et al. 2002, ApJ, 573, 184

Pooley, D., et al. 2002b, ApJ, 569, 405

Rosati, P., et al. 2002, ApJ, 566, 667

Spergel, D. N. 1991, Nature, 352, 221

Webbink, R. F., & Wickramasinghe, D. T. 2005, in ASP Conf. Ser. 330, The Astrophysics of Cataclysmic Variables and Related Objects, eds. J. M. Hameury & J. P. Lasota (San Francisco: ASP), 137

Table 1. Details of the Chandra observations of the selected globular clusters.

Obs. ID.	Detector	Start Date & Time (UTC)	Mode	Effective Exposure sec
M28 (NGC 6626)				
2683	ACIS-S	2002-09-09T16:55:03	VFAINT	14110
2684	ACIS-S	2002-07-04T18:02:19	VFAINT	12746
2685	ACIS-S	2002-08-04T23:46:25	VFAINT	13511
NGC 6440				
947	ACIS-S	2000-07-04T13:28:39	FAINT	23279
3360	ACIS-S	2001-08-18T20:04:32	FAINT	2511
3799	ACIS-S	2003-06-27T08:57:31	FAINT	24046
M62 (NGC 6266)				
2677	ACIS-S	2002-05-12T09:12:42	FAINT	62266
NGC 6752				
948	ACIS-S	2000-05-15T04:36:02	FAINT	29468
6612	ACIS-S	2006-02-10T22:48:48	VFAINT	37967
M5 (NGC 5904)				
2676	ACIS-S	2002-09-24T06:51:22	FAINT	44656
M13 (NGC 6205)				
5436	ACIS-S	2006-03-11T06:19:34	FAINT	26799
7290	ACIS-S	2006-03-09T23:01:13	FAINT	27895
M3 (NGC 5272)				
4542	ACIS-S	2003-11-11T16:33:18	VFAINT	9932
4543	ACIS-S	2004-05-09T17:26:32	VFAINT	10152
4544	ACIS-S	2005-01-10T08:54:31	VFAINT	9441
M71 (NGC 6838)				
5434	ACIS-S	2004-12-20T15:18:45	VFAINT	52446
M53 (NGC 5024)				
6560	ACIS-S	2006-11-13T18:32:22	VFAINT	24565
M4 (NGC 6121)				
946	ACIS-S	2000-06-30 04:24:23	VFAINT	25816

Table 2. Properties of 10 selected globular clusters.

Cluster Name	ρ_0[a]	$E(B-V)$[b]	distance	core radius	$L_{\rm limit}$[c]
	log $L_\odot$pc^{-3}		kpc	pc	erg s^{-1}
M28	4.73	0.40	5.5	0.38	3.5×10^{30}
NGC 6440	5.28	1.07	8.3	0.31	1.8×10^{31}
M62	5.14	0.47	6.9	0.36	7.1×10^{30}
NGC 6752	4.91	0.04	4.0	0.20	1.1×10^{30}
M5	3.91	0.03	7.5	0.92	6.7×10^{30}
M13	3.33	0.02	7.7	1.75	9.2×10^{30}
M3	3.51	0.01	10.4	1.66	1.4×10^{31}
M71	3.04	0.25	4.0	0.73	1.6×10^{30}
M53	3.05	0.02	17.8	1.86	1.3×10^{32}
M4	3.82	0.36	2.2	0.53	8.5×10^{29}

[a]Logarithm of central luminosity density

[b]Average foreground reddening

[c]Limiting luminosities inferred from the X-ray source detections

Table 3: X-ray spectral properties of the unresolved X-ray emission in the globular cluster cores.

Model [a]	χ^2_ν	D.O.F.	n^b_H 10^{21} cm^{-2}	Γ^c	$kT^d_{\rm BREMSS}$ keV	$kT^d_{\rm BB}$ keV	$L^e_{\rm PL}$ 10^{32} erg s^{-1}	$L^e_{\rm BREMSS}$ 10^{32} erg s^{-1}	$L^e_{\rm BB}$ 10^{31} erg s^{-1}
M28									
PL	0.83	25	$2.75^{+0.78}_{-0.84}$	$2.35^{+0.41}_{-0.25}$	-	-	$2.54^{+1.27}_{-0.62}$	-	-
BREMSS	0.82	25	$1.50^{+0.90}_{-0.76}$	-	$2.58^{+1.09}_{-0.75}$	-	-	$1.67^{+0.99}_{-0.62}$	-
PL+BB	0.84	25	2.2 (fixed)	$2.21^{+0.18}_{-0.23}$	-	0.18 (fixed)	$2.28^{+0.44}_{-0.56}$	-	< 2.21
BREMSS+BB	0.82	25	2.2 (fixed)	-	$2.68^{+0.87}_{-0.84}$	0.18 (fixed)	-	$1.66^{+0.95}_{-0.67}$	$2.21^{+2.19}_{-2.21}$
NGC 6440									
PL	0.39	4	5.9 (fixed)	$2.04^{+0.50}_{-0.46}$	-	-	$2.00^{+1.71}_{-0.76}$	-	-
BREMSS	0.44	4	5.9 (fixed)	-	$3.06^{+6.18}_{-1.25}$	-	-	$1.57^{+1.51}_{-0.74}$	-
PL+BB	0.51	3	5.9 (fixed)	$1.83^{+0.69}_{-0.56}$	-	0.18 (fixed)	$1.77^{+3.02}_{-1.33}$	-	$3.61^{+11.49}_{-3.61}$
BREMSS+BB	0.44	4	5.9 (fixed)	-	3.06 (fixed)	0.18 (fixed)	-	$1.54^{+0.27}_{-0.33}$	$1.19^{+7.49}_{-1.19}$
M62									
PL	0.43	8	< 0.52	$1.54^{+0.22}_{-0.16}$	-	-	$1.50^{+0.62}_{-0.36}$	-	-
BREMSS	0.58	8	< 0.35	-	$9.23^{+17.50}_{-4.10}$	-	-	$1.41^{+0.26}_{-0.27}$	-
PL+BB	0.34	8	2.6 (fixed)	$1.03^{+0.17}_{-0.18}$	-	0.18 (fixed)	$1.50^{+1.46}_{-0.74}$	-	$8.19^{+1.97}_{-2.45}$
BREMSS+BB	0.53	9	2.6 (fixed)	-	9.23 (fixed)	0.18 (fixed)	-	1.33 ± 0.19	6.15 ± 1.58
NGC 6752									
PL	0.95	7	0.22 (fixed)	$1.94^{+0.39}_{-0.36}$	-	-	$0.15^{+0.08}_{-0.04}$	-	-
BREMSS	0.89	7	0.22 (fixed)	-	$2.38^{+3.06}_{-1.00}$	-	-	$0.12^{+0.11}_{-0.06}$	-
PL+BB	0.95	7	0.22 (fixed)	1.94 (fixed)	-	0.18 (fixed)	$0.15^{+0.02}_{-0.04}$	-	< 0.23
BREMSS+BB	1.04	6	0.22 (fixed)	-	$2.38^{+3.08}_{-1.00}$	0.18 (fixed)	-	$0.12^{+0.11}_{-0.07}$	< 0.33

[a] PL=Power-law; BREMSS=Thermal bremsstrahlung; BB=Blackbody

[b] Hydrogen column density

[c] X-ray photon index

[d] $kT_{\rm BB}/kT_{\rm BREMSS}$ is the temperature of the black body/thermal bremsstrahlung model.

[e] $L_{\rm PL}/L_{\rm BREMSS}/L_{\rm BB}$ is the absorption-corrected luminosity inferred from the power-law/thermal bremsstrahlung/black body component.

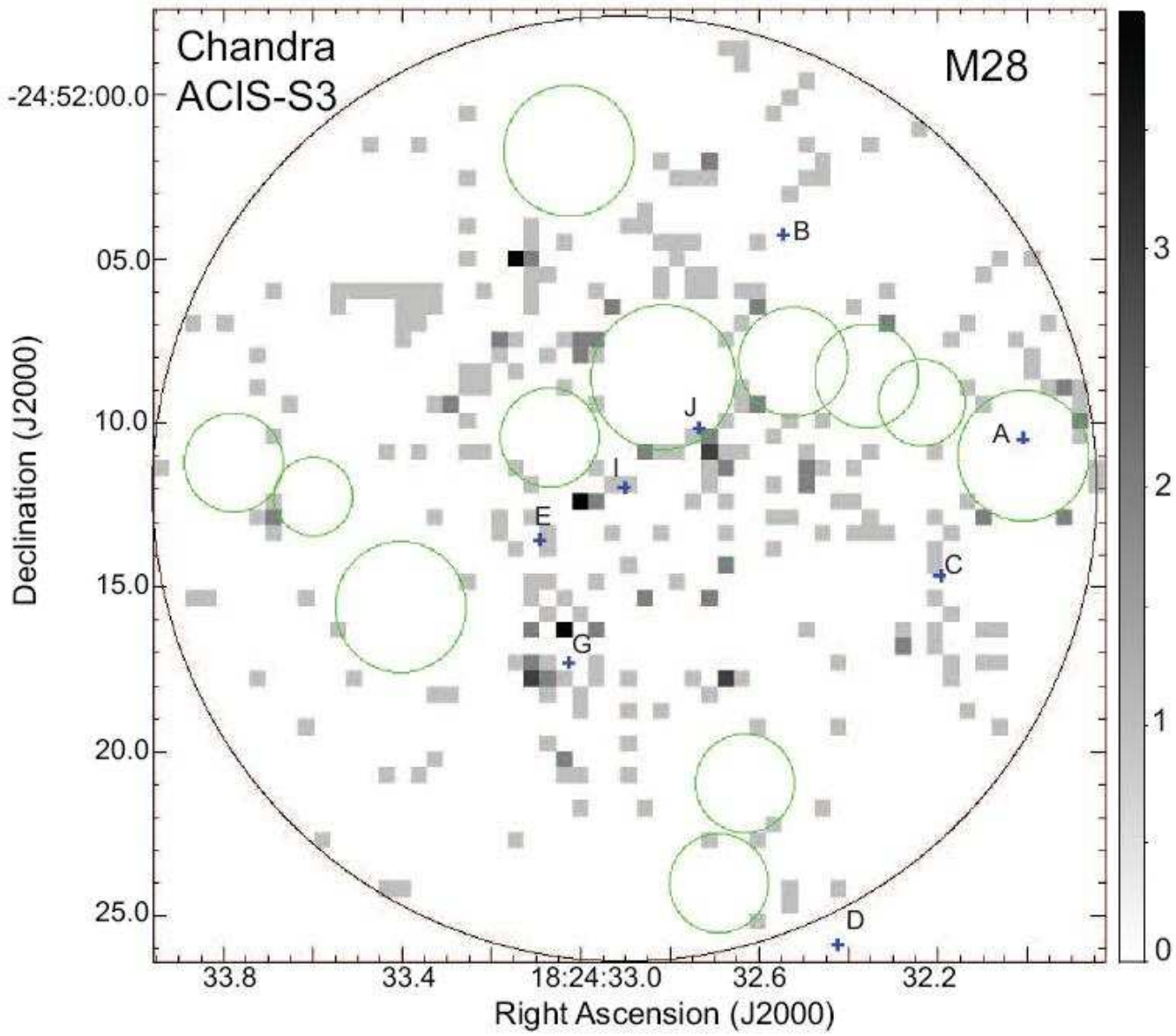

Fig. 1.— The raw X-image of the unresolved emission within the core radius of M28 as observed by Chandra ACIS-S3 CCD in $0.3 - 8$ keV. The excluded regions of the detected point sources are illustrated as green circles. The black circle indicates the region of 1 core radius centered at the optical center. The image is created by merging all three ACIS observations. The radio timing positions of eight MSPs in the field-of-view of this image are illustrated by the crosses. The count scale in each pixel is illustrated by the grey-scale bar.

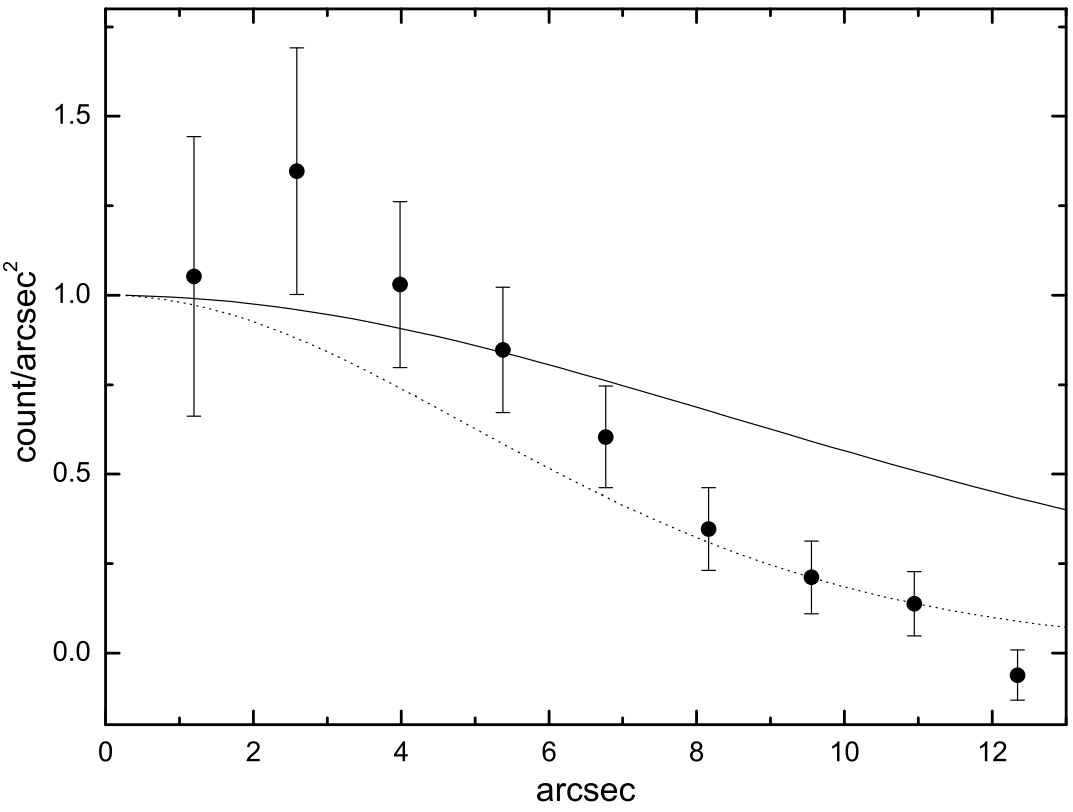

Fig. 2.— The radial brightness profile of the unresolved emission within the core radius of M28 as observed by Chandra ACIS-S3 CCD in $0.3 - 8$ keV. The solid line and the dotted line (with the vertical quantity in arbitrary units) represent the best-fit projected surface density profile of the detected point sources and the profile with the parameters stretched to 1σ uncertainties reported by Becker et al. (2003) respectively.

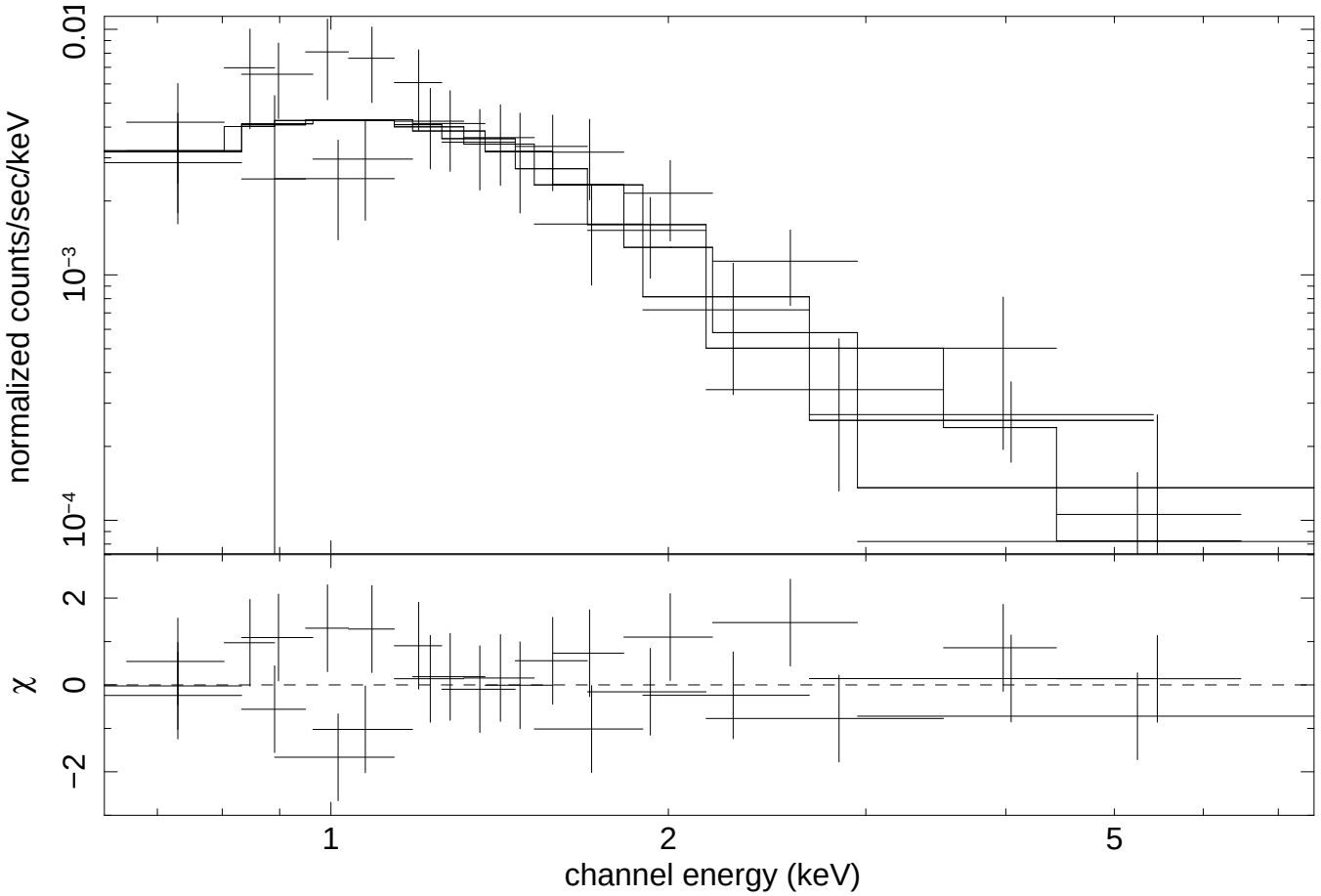

Fig. 3.— Energy spectrum of the unresolved X-rays in the core of M28, as observed with ACIS-S3 detectors and fitted to an absorbed power-law model (*upper panel*) and contribution to the χ^2 fit statistic (*lower panel*).

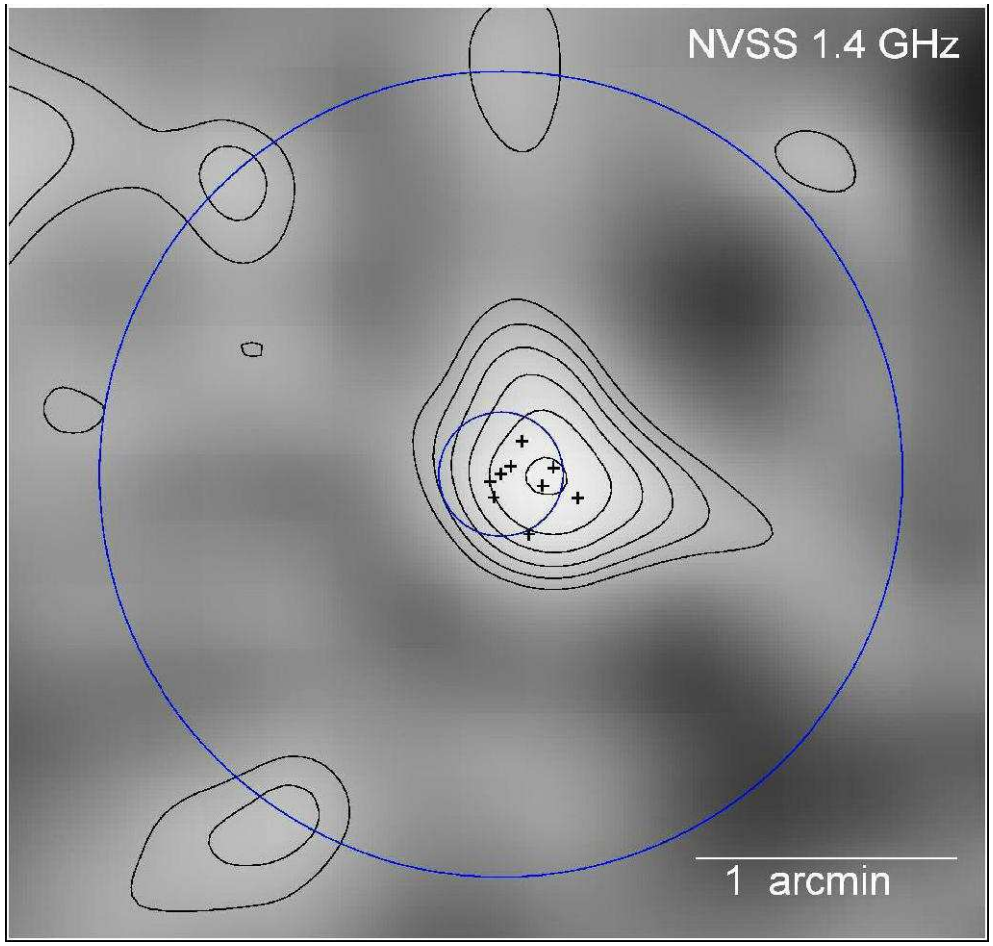

Fig. 4.— The 1.4 GHz NVSS image of the field around M28. Top is north and left is east. The radio pulsar positions are indicated by black crosses. The radio contours are at the levels between 0.5 mJy/beam−2 mJy/beam. The blue circles are centered at the optical center of the cluster with the radii equal to the core radius (small) and the half-mass radius (large).